HHS Public Access

Author manuscript

J Am Chem Soc. Author manuscript; available in PMC 2023 May 04.

Published in final edited form as:

J Am Chem Soc. 2022 May 04; 144(17): 7871–7880. doi:10.1021/jacs.2c02058.

Fluorogenic cyclopropenones for multi-component, real-time imaging

Tyler K. Heiss[†], **Robert S. Dorn**[†,∇], **Andrew. J. Ferreira**[†,∇], **Anna C. Love**[†], **Jennifer A. Prescher**[*,†,‡,§]

[†]Departments of Chemistry, University of California, Irvine, California 92697, United States.

[‡]Molecular Biology & Biochemistry, University of California, Irvine, California 92697, United States.

[§]Pharmaceutical Sciences, University of California, Irvine, California 92697, United States.

Abstract

Fluorogenic bioorthogonal reactions enable biomolecule visualization in real time. These reactions comprise reporters that “light up” upon reaction with complementary partners. While the spectrum of fluorogenic chemistries is expanding, few transformations are compatible with live cells due to cross-reactivities or insufficient signal turn-on. To address the need for more suitable transformations for cellular imaging, we developed a fluorogenic reaction featuring cyclopropenone reporters and phosphines. The transformation involves regioselective activation and cyclization of cyclopropenones to form coumarin products. With optimal probes, the reaction provides >1,600-fold signal turn-on, one of the highest fluorescence enhancements reported to date. The bioorthogonal motifs were evaluated *in vitro* and in cells. The reaction was also found to be compatible with other common fluorogenic transformations, enabling multi-component imaging. Two cellular targets were visualized simultaneously, a first for fluorogenic bioorthogonal chemistries. Collectively, these data suggest that the cyclopropenone-phosphine reaction will bolster efforts to track biomolecule targets in their native settings

Graphical Abstract

[*]Correspondence should be addressed to jpresche@uci.edu.

[∇]Author Contributions

R.S.D. and A.J.F. contributed equally.

Supporting Information.

The Supporting Information is available free of charge on the ACS Publications website at DOI:

Experimental details, spectroscopic data for new compounds, additional images, Figures S1–S13, Scheme S1–S2, and Table S1 (PDF).

Simultaneous orthogonal fluorogenic reactions (CpO-PR3, green) (Movie S1) (AVI).

Simultaneous orthogonal fluorogenic reactions (**TCO-Tz**, magenta) (Movie S2) (AVI).

Simultaneous orthogonal fluorogenic reactions (CpO-PR3 green, **TCO-Tz** magenta) (Movie S3) (AVI).

The authors declare no competing financial interest.

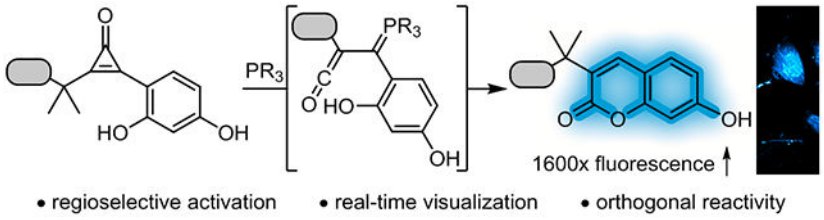

INTRODUCTION

Efforts to visualize cellular biomolecules have long relied on fluorescent probes.[1-3] Such imaging agents can be appended to targets via several methods, including the bioorthogonal chemical reporter stategy.[4-7] In this approach, biomolecules are outfitted with a unique chemical handle via probe metabolism. A fluorophore is covalently attached in a subsequent step using selective (i.e., bioorthogonal) chemistry. Such reactions typically require excess probe to boost labeling rates. Unreacted fluorophores must be removed prior to visualization to avoid background signal. Dye removal can be challenging in some applications and preclude the observation of dynamic cellular events.

Fluorogenic bioorthogonal reactions offer a more facile means to visualize cellular features.[8-10] In these transformations, non-emissive reporters “light up” only upon reaction with complementary reagents (Figure 1A). The detection probe can be used in excess to drive the reaction, with no need to remove unbound reagent. Such wash-free reactions are attractive for live cell microscopy and related applications.

Several fluorogenic bioorthogonal chemistries have been developed for *in vitro* labeling, but few can be deployed in living cells.[8] These latter applications require both fast and exquisitely biocompatible reactions with robust fluorescence enhancements. Arguably the most popular fluorogenic transformations comprise a singular reaction type: the inverse electron-demand Diels–Alder (IEDDA) cycloaddition of strained dienophiles (e.g. *trans*-cyclooctene, **TCO**) and electron-deficient dienes (e.g. 1,2,4,5-tetrazine, **Tz**). These ligations are fast, cell-compatible, and can illuminate biomolecules in real time.[11-18] Existing fluorogenic IEDDA reactants cannot be administered together, though, owing to cross reactivity issues. Multiplexing with other bioorthogonal reagents has also been complicated by slow rates and poor signal turn-ons. Consequently, real-time imaging of multiple cellular targets remains challenging.[19-22] Visualizing dynamic multi-component processes[23,24] requires biocompatible, fluorogenic motifs with unique reactivity profiles.

To address this void, we aimed to develop a new fluorogenic reaction based on a recently reported bioorthogonal reagent, the cyclopropenone (CpO). CpO motifs are small, stable, and genetically encodable.[25,26] They react with triarylphosphine nucleophiles to form α,β-unsaturated carbonyl products via ketene-ylide intermediates.[26,27] Ketene-ylides are versatile electrophiles for biomolecule tagging, crosslinking, and natural product synthesis.[25,26,28-30]

We further recognized that ketene-ylides could be intercepted to form fluorescent products (Figure 1B). Therefore, in this work, we employed proximal phenol nucleophiles

to yield coumarin fluorophores (Figure 1C). A suite of sterically modified CpO reagents was prepared and screened with a panel of phosphines to identify suitable fluorogenic reactants. Successful coumarin formation was found to be highly dependent on regioselective activation of the CpO scaffold. The most optimal reagents provided robust signal enhancement (~1,600-fold). We further synthesized conjugatable CpO probes for biomolecule modification. These reagents enabled the detection of biological targets *in vitro* and in live cells. The fluorogenic CpO reaction is also orthogonal to IEDDA cycloadditions, and we capitalized on this compatibility to visualize cellular targets in tandem. The versatility of the fluorogenic CpO transformation should enable a range of biomolecule tracking experiments in physiological settings.

RESULTS AND DISCUSSION

We envisioned leveraging the unique reactivity of bioorthogonal cyclopropenones to form coumarin adducts. Coumarin dyes are attractive for biological application due to their small size, photostability, and versatility.[1, 31-37] Some functionalized cyclopropenones are known to form coumarins upon prolonged heating.[38] The reaction involves ketene generation and subsequent lactonization. However, this method is inefficient due to several competing pathways. Furthermore, strong heating is required; such conditions are not translatable to biological settings.

We surmised that the requisite ketene intermediates could be accessed under more biocompatible conditions (i.e., using bioorthogonal phosphines).[28] In this strategy, phosphine addition at C2 would yield the desired ketene (Figure 2). If a proximal phenol nucleophile was present, the intermediate could be intramolecularly trapped to forge the α,β-unsaturated lactone framework of coumarin fluorophores. A competing pathway was also envisioned—phosphine addition at C3. This reaction would provide non-emissive benzofuran-2(3H)-one adducts. Successful coumarin formation therefore hinged on regioselective phosphine addition at C2.

We hypothesized that the desired C2 addition could be achieved using CpO reagents with large modifications at C3 (Figure 3A). To test this idea, a panel of CpO probes (**1a**–**c**) comprising bulky C3 substituents was designed. The molecules were accessed from 2-iodophenyl acetate (**S1**) via Sonogashira coupling followed by difluorocarbene insertion and hydrolysis (Scheme S1).[39,40] Upon isolation, the probes were reacted with triphenylphosphine (PPh_3, **4** Figure 3B), a widely available bioorthogonal reagent known to activate CpO motifs.[27] Unfortunately, when CpO scaffolds **1a**–**b** were treated with PPh_3, only the undesired furanone adducts (**3a**–**b**) were formed (Figures 3c and S1-S2). The most sterically encumbered CpO **1c** afforded some of the desired coumarin (**2c**), but the reaction was very low yielding, nonselective, and slow (Figures 3c and S3).

To identify a more robust trigger for coumarin formation, we surveyed additional phosphine scaffolds. We surmised that both phosphine size and nucleophilicity would play key roles, with the former parameter influencing regioselective activation and the latter dictating the overall rate.[41] With these considerations in mind, cyclohexyldiphenylphosphine ($PCyPh_2$, **5**) and 1,3,5-triaza-7-phosphaadamantane (PTA, **6**) were selected as model bulky and compact

phosphines, respectively. Both of these reagents are also sufficiently nucleophilic and known to be compatible with aqueous solution.[30, 42,43] Phosphines **5**–**6** were incubated with CpOs **1a**–**c**, and the distributions of cyclized products were determined using both NMR and LC-MS analyses. When CpOs **1a**–**b** were treated with either phosphine, the undesired 5-membered lactones (**3a**–**b**) were still the major products (Figures S1-S2). By contrast, no furanone was observed when CpO **1c** was treated with $PCyPh_2$ (**5**, Figure S3). The *tert*-butyl group likely blocked phosphine attack at C3, giving rise to the desired adduct. No coumarin formation was observed when CpO **1c** was treated with PTA (**6**), though, suggesting that phosphine size and electronics also play a role in the observed product distribution. The exact mechanism governing phosphine addition remains unclear and warrants further investigation.

To further improve the fluorescent output of the reaction, we added another electron donating group to the core of CpO **1c** (Figure 4A).[45] The resulting probe (CpO **7**) featured the *tert*-butyl group required for regioselective activation, along with a resorcinol appendage to enhance product emission. We hypothesized that CpO **7** would react with phosphine activators to form 7-hydroxycoumarin fluorophores, brighter and well-vetted fluorescent dyes.[33] Fluorogenic CpO probe **7** was prepared via a similar synthetic route as analogs **1a**–**c** (Scheme S2). In brief, acetate-protected 2-iodoresorcinol was ligated with 3,3-dimethylbutyne via Sonogashira coupling. Difluorocarbene insertion and subsequent hydrolysis ultimately delivered the desired probe (**7**).

With the fluorogenic CpO in hand, we examined the activation-cyclization sequence in aqueous solution. Until this point, the reaction had only been performed in organic solvents devoid of competing nucleophiles for ketene trapping. Intermolecular hydrolysis is possible in aqueous environments, though, which would diminish fluorophore formation. To evaluate the reaction in buffer, we first sulfonated phosphine **5** to give cyclohexyldiphenylphosphine disulfonate (**CyDPPDS**, **8**). The sulfonate groups were selected to impart water solubility without sacrificing phosphine reactivity.[28] When phosphine **8** and fluorogenic CpO **7** were combined in buffer, coumarin **9** formed exclusively (Figure 4A). No competing intermolecular hydrolysis was observed, indicating that cyclization is favorable even in aqueous solution (Figure S4). Coumarins are also susceptible to quenching by phosphine probes.[46,47] However, we did not observe any change in fluorescence when coumarin **9** was subjected to excess phosphine (Figure S5).

We next measured the photophysical properties of CpO **7** and its cyclized products. A synthetic standard of coumarin **9** was prepared, along with the off-target benzofuranone **10** (Figure 4A). All compounds (**7**, **9**–**10**) absorbed light to a similar extent (Figure 4B), but exhibited vastly different emission profiles (Figure 4C). Both CpO **7** and the off-target product **10** were poor emitters. By contrast, the desired coumarin **9** exhibited a 1,600-fold increase in fluorescence compared to the starting CpO probe (**7**, Figure 4D). This fluorescence “turn-on” is among the largest enhancements reported to date and is on par with several transformations previously applied in live-cell imaging.[14,15,17] The brightness of coumarin **9** was also similar to the known fluorophore, 7-hydroxycoumarin. We further determined the second-order rate constant for the fluorogenic transformation (k_2 = 0.044

M^{-1} s^{-1}, Figure 4E). The reaction is slower than the most popular IEDDA reactions used in cellular settings, but comparable to other fluorogenic transformations used *in vitro*.[16, 48-50]

We next aimed to apply the fluorogenic reaction for biomolecule detection. We initially pursued a CpO reagent (**14**) equipped with a nucleophilic handle for facile biomolecule attachment. Aryl iodide **11** and protected propargyl alcohol **12** were first ligated via Sonogashira cross-coupling (Scheme 1A). When the product (**13**) was subjected to the key difluorocarbene insertion reaction, though, prohibitively low quantities of CpO (**14**) were obtained, likely due to the electron-deficient nature of the alkyne (σ_p = +0.31 for -OAc, Figure S6).[29, 39] The more electron-rich alkyne **15** (σ_p = −0.27 for -OMe) provided improved CpO yields (Scheme 1B),[51,52] and subsequent acetal cleavage delivered tertiary alcohol **16**. Initial attempts to activate **16** for bioconjugation were unsuccessful, as both the CpO and *gem*-dimethyl moieties blocked reactivity of the hydroxy group (Scheme 1B, Table S1).[53] To circumvent this issue, a short linker was installed between the *gem*-dimethyl group and conjugation site (Scheme 1C). Aryl bromide **18** was thus coupled with elongated alkyne **19**, and the product was converted to an activated ester.[54-56] Alkyne **19** also required a protecting group to prevent lactonization during the cross-coupling step (Figure S7).[57,58] PFP-ester **20** was ultimately subjected to carbene insertion, hydrolysis, and acidic deprotection to deliver the desired **FluorCpO** probe (**21**).[35]

To evaluate **FluorCpO** in a biological context, we performed the fluorogenic reaction on a model protein *in vitro*. Hen egg white lysozyme (HEWL) was non-specifically functionalized with **FluorCpO** motifs (Figure S8, 1–6 modifications). The conjugates were then treated with phosphine **8** and analyzed via gel electrophoresis (Figure 5A). Fluorophore formation was both dose- and time-dependent (Figure 5B-C). Fluorescence enhancement was observed within 5 min of phosphine treatment, and the reaction was completed in 90 min. Catalytic amounts of phosphine **8** were also sufficient for fluorescence turn-on. The fluorogenic CpO reaction is further compatible with live cells. A549 cells were non-specifically labeled with **FluorCpO** (**21**).[53] The cultures were then treated with phosphine **8** (Figure 6A). Subsequent imaging was performed via confocal microscopy. As shown in Figure 6B, robust coumarin fluorescence was observed within 30 min. In the absence of either reagent, background signal was not observed. These results indicate that the fluorogenic CpO reaction is well-suited for cellular application.

We further investigated the platform for multi-component labeling. Visualizing multiple targets requires mutually orthogonal reactions, but only a handful of bioorthogonal transformations are compatible with one another.[20,22,59] The fluorogenic CpO-phosphine transformation is mechanistically distinct and likely compatible with the most commonly applied fluorogenic reaction, the IEDDA ligation (Figure 7A).[11,12,15,17] To investigate this possibility, we performed reactions on modified proteins bearing either **TCO** or **FluorCpO** handles. **TCO** handles were nonspecifically installed on BSA as a model protein (**TCO-BSA**, Figure S9), and **FluorCpO** moieties were conjugated to HEWL. The protein conjugates were then subjected to the complementary fluorogenic triggers (**Tz-BODIPY** or phosphine **8**). Strong fluorescent signals were detected when either protein conjugate was incubated with its matching partner in isolation (Figure 7B). When the two transformations were performed simultaneously in lysate, both protein targets were successfully visualized.

No cross-reactivities were observed, highlighting the biocompatibility and orthogonality of these two reactions. The resulting fluorophores were also easily spectrally resolved, setting the stage for tandem imaging.

We next combined the fluorogenic CpO and **TCO**-**Tz** reactions for multiplexed imaging. To modify cellular proteins with **TCO** groups, we leveraged a previously established SNAP-tag labeling method.[60-62] We generated a mammalian cell line stably expressing a mitochondrial localized SNAP-tag reporter (HEK MitoSNAP). SNAP-tagged proteins were labeled with a **TCO**-benzylguanine probe (**TCO–SNAP-tag**) and visualized via reaction with **Tz-BODIPY**. Fluorescence enhancement was only observed in the presence of both the **TCO** and **Tz** reagents (Figure S10). BODIPY fluorescence also colocalized with a mitochondrial stain (Figure S10).

Having verified the selectivity of both transformations, the fluorogenic reactions were employed simultaneously to image biomolecule targets in live cells. In an initial model system, MitoSNAP HEK cells were labeled with **TCO** and **FluorCpO** reporters (Figure 8A). In the absence of the complementary tetrazine and phosphine probes, minimal fluorescence was observed (Figure 8B). By contrast, when the dual labeled cells were incubated with **Tz-BODIPY** and phosphine **8**, robst fluorescent signals were observed from both reactions within 5 minutes (Figure 8C). The signals were monitored simultaneously and increased in intensity over 90 min (Figures 8C-D, movies S1-S3).

The fluorogenic reactions were further used to examine the biological impacts of a sterol metabolite.[17,23-24] Sterols play essential roles in eukaryotes, both as membrane components and signaling molecules. Key questions remain, though, regarding their cellular localization and function. Since sterols cannot be tracked with classic genetic tags and often exert their effects on short time scales,[63] they are attractive targets for real-time imaging with fluorogenic bioorthogonal reactions.

To showcase the potential of **FluorCpO** in this context, we focused on deoxycholic acid (DCA) and related metabolites—known signaling molecules[64] that modulate a variety of cellular processes, including Golgi membrane dynamics.[65-67] Additional insights into DCA localization and function could potentially be gained via live cell imaging. Toward this end, we synthesized a **FluorCpO**-modified analog of deoxycholic acid (**DCA-FluorCpO**, Figures 9 and S11). The analog was based on related C24-modified sterols,[68-71] and imaging experiments revealed probe localization to cellular membranes (Figure S12). To examine the effects of the sterol on live cells, we employed a TCO-modified ceramide derivative (**TCO-Cer**, Figure S13). **TCO-Cer** has been previously used to track Golgi dynamics, and unlike other labeling agents, can be visualized over extended time periods.[72] **DCA-FluorCpO** and **TCO-Cer** were mixed and added to live cell cultures (Figure 9A). No background signal was observed in the absence of the corresponding bioorthogonal triggers (Figure 9B). When **BODIPY-Tz** and phosphine **8** were added, though, robust fluorecence was detected (Figure 9C). **DCA-FluorCpO** partitioning into the Golgi was observed, and in some cases, disrupted organelles appeared, consistent with observations from fixed cells.[73,74] These experiments highlight the utility of fluorogenic reactions for real-time imaging and set the stage for further biological application.

CONCLUSION

In conclusion, we developed a new fluorogenic reaction of CpO and phosphine probes. This reaction converts CpO reagents to fluorescent coumarin products via regioselective activation with phosphine nucleophiles and subsequent cyclization. The coumarin products are significantly more fluorescent than the non-emissive starting materials, and the enhancement is among the highest reported for bioorthogonal fluorogenic reactions to date (1,600-fold).

We also synthesized a bioconjugatable CpO reagent and applied this probe to successfully visualize biological targets *in vitro* and in live cells. Biomolecules were detected within 5 min of phosphine addition, without the need for washing steps. Additionally, the fluorogenic CpO reaction is compatible with the inverse electron-demand Diels–Alder (IEDDA) cycloaddition reaction. We capitalized on this orthogonality to simultaneously image two metabolites in real-time, a first for fluorogenic bioorthogonal chemistries.

We anticipate that the CpO-phosphine reaction will be translatable to a broad range of cellular targets. **FluorCpO** reagents are modular and can be ligated to a variety of biomolecule classes. The fluorogenic transformation is useful as a standalone reaction or in combination with other bioorthogonal chemistries. Orthogonal fluorogenic reagents offer new avenues for multi-metabolite imaging, among other applications.[75] In the future, we plan to further tune the **FluorCpO** scaffold to produce emission profiles across the visible spectrum.[76-78] Such probes will add to the growing bioorthogonal toolkit and enable new pursuits.

Supplementary Material

Refer to Web version on PubMed Central for supplementary material.

ACKNOWLEDGMENTS

This work was supported by the U.S. National Institutes of Health (R01 GM126226 to J.A.P.), the Alfred P. Sloan Foundation (J.A.P.), and the Chan Zuckerberg Initiative (J.A.P.). A.J.F. was supported by a George Hewitt Medical Research Postdoctoral Fellowship. We thank the Dong, Blum, Heyduk, Weiss, Nowick, Chamberlin, and Spitale laboratories for providing reagents and equipment. We also thank Philip Dennison (UCI) for assistance with NMR experiments, and Felix Grün (UCI) and Benjamin Katz (UCI) for assistance with mass spectrometry experiments. We thank Dima Fishman (UCI) and the Laser Spectroscopy labs for providing instrumentation for absorbance and fluorescence measurements. This study was made possible in part through access to the Optical Biology Core Facility of the Developmental Biology Center, a shared resource supported by the Cancer Center Support Grant (CA-62203) and Center for Complex Biological Systems Support Grant (GM-076516) at the University of California, Irvine. BioRender (https://biorender.com/) was used to prepare some figures in this text. Last, we thank members of the Prescher laboratory for manuscript edits and helpful discussions.

REFERENCES

1. Lavis LD; Raines RT Bright Building Blocks for Chemical Biology. ACS Chem. Biol 2014, 9, 855–866. [PubMed: 24579725]
2. van de Linde S; Heilemann M; Sauer M Live-Cell Super-Resolution Imaging with Synthetic Fluorophores. Annu. Rev. Phys. Chem 2012, 63, 519–540. [PubMed: 22404589]
3. Specht EA; Braselmann E; Palmer AE A Critical and Comparative Review of Fluorescent Tools for Live-Cell Imaging. Annu. Rev. Physiol 2017, 79, 93–117. [PubMed: 27860833]

4. Sletten EM; Bertozzi CR Bioorthogonal Chemistry: Fishing for Selectivity in a Sea of Functionality. Angew. Chem. Int. Ed 2009, 48, 6974–6998.
5. McKay CS; Finn MG Click Chemistry in Complex Mixtures: Bioorthogonal Bioconjugation. Cell Chem. Biol 2014, 21, 1075–1101.
6. Lang K; Chin JW Cellular Incorporation of Unnatural Amino Acids and Bioorthogonal Labeling of Proteins. Chem. Rev 2014, 114, 4764–4806. [PubMed: 24655057]
7. Nguyen SS; Prescher JA Developing Bioorthogonal Probes to Span a Spectrum of Reactivities. Nat. Rev. Chem 2020, 4, 476–489. [PubMed: 34291176]
8. Shieh P; Bertozzi CR Design Strategies for Bioorthogonal Smart Probes. Org. Biomol. Chem 2014, 12, 9307–9320. [PubMed: 25315039]
9. Wu H; Devaraj NK Advances in Tetrazine Bioorthogonal Chemistry Driven by the Synthesis of Novel Tetrazines and Dienophiles. Acc. Chem. Res 2018, 51, 1249–1259. [PubMed: 29638113]
10. Tian Y; Lin Q Fitness Factors for Bioorthogonal Chemical Probes. ACS Chem. Biol 2019, 14, 2489–2496. [PubMed: 31769957]
11. Lang K; Davis L; Wallace S; Mahesh M; Cox DJ; Blackman ML; Chin JW Genetic Encoding of Bicyclononynes and *trans*-Cyclooctenes for Site-Specific Protein Labeling in Vitro and in Live Mammalian Cells via Rapid Fluorogenic Diels–Alder Reactions. J. Am. Chem. Soc 2012, 134, 10317–10320. [PubMed: 22694658]
12. Wu H; Alexander SC; Devaraj NK A Bioorthogonal Near-Infrared Fluorogenic Probe for mRNA Detection. J. Am. Chem. Soc 2016, 138, 11429–11432. [PubMed: 27510580]
13. Werter R; Yserentant K; Braun F; Kaltwasser N; Popp C; Baalmann M; Herten D-P; Wombacher R Live-Cell Localization Microscopy with a Fluorogenic and Self-Blinking Tetrazine Probe. Angew. Chem. Int. Ed 2020, 59, 804–810.
14. Lee Y; Cho W; Sung J; Kim E; Park SB Monochromophoric Design Strategy or Tetrazine-Based Colorful Bioorthogonal Probes with a Single Fuorescent Core Skeleton. J. Am. Chem. Soc 2018, 140, 974–978. [PubMed: 29240995]
15. Carlson JCT; Meimetis LG; Hilderbrand SA; Weissleder R BODIPY-Tetrazine Derivatives as Superbright Bioorthogonal Turn-On Probes. Angew. Chem. Int. Ed 2013, 52, 6917–6920.
16. Yang J; Šečkutė J; Cole CM; Devaraj NK Live-Cell Imaging of Cyclopropene Tags with Fluorogenic Tetrazine Cycloadditions. Angew. Chem. Int. Ed 2012, 51, 7476–7479.
17. Liang D; Wu K; Tei R; Bumpus TW; Ye J; Baskin JM A Real-Time, Click Chemistry Imaging Approach Reveals Stimulus-Specific Subcellular Locations of Phospholipase D Activity. Proc. Natl. Acad. Sci 2019, 116, 15453–15462. [PubMed: 31311871]
18. Wieczorek A; Werther P; Euchner J; Wombacher R Green- to Far-Red-Emitting Fluorogenic Tetrazine Probes – Synthetic Access and No-Wash Protein Imaging Inside Living Cells. Chem. Sci 2017, 8, 1506–1510. [PubMed: 28572909]
19. Devaraj NK The Future of Bioorthogonal Chemistry. ACS Cent. Sci 2018, 4, 952–959. [PubMed: 30159392]
20. Smeenk MLWJ; Agramunt J; Bonger KM Recent Developments in Bioorthogonal Chemistry and the Orthogonality Within. Curr. Opin. Chem. Biol 2021, 60, 79–88. [PubMed: 33152604]
21. Hu Y; Schomaker JM Recent Developments and Strategies for Mutually Orthogonal Bioorthogonal Reactions. ChemBioChem 2021, 22, 3254–3262. [PubMed: 34261195]
22. Patterson DM; Prescher JA Orthogonal Bioorthogonal Chemistries. Curr. Opin. Chem. Biol 2015, 28. [PubMed: 26615565]
23. Chu L; Tyson J; Shaw JE; Rivera-Molina F Koleske AJ; Schepartz A; Toomre DK Two-color Nanoscopy of Organelles for Extended Times with HIDE Probes. Nat. Commun 2020, 11, 4271. [PubMed: 32848153]
24. Tamura T; Fujisawa A; Tsuchiya M; Schen Y; Nagao K; Kawano S; Tamura Y; Endo T; Umeda M; Hamachi I Organelle Membrane-specific Chemical Labeling and Dynamic imaging in Living Cells. Nat. Chem. Biol 2020, 16, 1361–1367. [PubMed: 32958953]
25. Shih H-W; Prescher JA A Bioorthogonal Ligation of Cyclopropenones Mediated by Triarylphosphines. J. Am. Chem. Soc 2016, 137, 10036–10039.

26. Row RD; Shih H-W; Alexander AT; Mehl RA; Prescher JA Cyclopropenones for Metabolic Targeting and Sequential Bioorthogonal Labeling. J. Am. Chem. Soc 2017, 139, 7370–7375. [PubMed: 28478678]
27. Hamada A; Takizawa T Reactions of Diphenylcyclopropenone with Trivalent Phosphorous Compounds. Chem. Pharm. Bull 1975, 23, 2933–2938.
28. Heiss TK; Dorn RS; Prescher JA Bioorthogonal Reactions of Triarylphosphines and Related Analogues. Chem. Rev 2021, 121, 6802–6849. [PubMed: 34101453]
29. Nguyen SN; Ferreira AF; Long ZG; Heiss TK; Dorn RS; Row RD; Prescher JA Butenolide Synthesis from Functionalized Cyclopropenones. Org. Lett 2019, 21, 8695–8699. [PubMed: 31622107]
30. Row RD; Nguyen SS; Ferreira AJ; Prescher JA Chemically Triggered Crosslinking with Bioorthogonal Cyclopropenones. Chem. Commun 2020, 56, 10883–10886.
31. Klán P; Šolomek T; Bochet CG; Blanc A; Givens R; Rubina M; Popik V; Kostikov A; Wirz J Photoremovable Protecting Groups in Chemistry and Biology: Reaction Mechanisms and Efficacy. Chem. Rev 2013, 113, 119–191. [PubMed: 23256727]
32. Liu J; Hemphill J; Samanta S; Tsang M; Dieters A Genetic Code Expansion In Zebrafish Embryos and its Application to Optical Control of Cell Signaling. J. Am. Chem. Soc 2017, 139, 9100–9103. [PubMed: 28657738]
33. Uttamapinant C; White KA; Baruah H; Thompson S; Fernandez-Suarez M; Puthenveetil S; Ting AY A Fluorophore Ligase for Site-Specific Protein Labeling Inside Living Cells. Proc. Natl. Acad. Sci 2010, 107, 10914–10919. [PubMed: 20534555]
34. Aronoff MR; Hiebert P; Hentzen NB; Werner S; Wennemers H Imaging and Targeting LOX-Mediated Tissue Remodeling With A Reactive Collagen Peptide. Nat. Chem. Biol 2021, 17, 865–871. [PubMed: 34253910]
35. Luo J; Uprety R; Naro Y; Chou C; Nguyen DP; Chin JW; Deiters A Genetically Encoded Optochemical Probes for Simultaneous Fluorescence Reporting and Light Activation of Protein Function with Two-Photon Excitation. J. Am. Chem. Soc 2014, 136, 15551–15558. [PubMed: 25341086]
36. Wang J; Xie J; Schultz PG A Genetically Encoded Fluorescent Amino Acid. J. Am. Chem. Soc 2006, 128, 8738–8739. [PubMed: 16819861]
37. Cao D; Liu Z; Verwilst P; Koo S; Jangjili P; Kim JS; Lin W Coumarin-Based Small-Molecule Fluorescent Chemosensors. Chem. Rev 2019, 119, 10403–10519. [PubMed: 31314507]
38. Eicher T; Scheider V Synthesis and Properties of *o*-Hydroxypenyl and *o*-Acetylaminophenyl Substituted Cyclopropenones. A Novel Thermal Transformation of Functionalized Diarylcyclopropenones. Synthesis 1989, 5, 372–378.
39. Wang F; Luo T; Hu J; Wang Y; Krishnan HS; Jog PV; Ganesh SK; Prakash GK; Olah GA Synthesis of *gem*-Difluorinated Cyclopropanes and Cyclopropenes: Trifluoromethyltrimethylsilane as a Difluorocarbene Source. Angew. Chem. Int. Ed 2011, 50, 7153–7157.
40. García-Domínguez A; West TH; Primozic JJ; Grant KM; Johnston CP; Cumming GG; Leach AG; Lloyd-Jones GC Difluorocarbene Generation from $TMSCF_3$: Kinetics and Mechanism of NaI-Mediated and Si-Induced Anionic Chain Reactions. J. Am. Chem. Soc 2020, 142, 14649–14663. [PubMed: 32786804]
41. Musina EI; Balueva AS; Karasik AA Phosphines: Preparation, Reactivity, and Applications. Organophosphorous Chem. 2019, 48, 1–63.
42. Henderson WA; Buckler SA The Nucleophilicity of Phosphines. J. Am. Chem. Soc 1960, 82, 5794–5800.
43. Frost BJ; Mebi CA Aqueous Organometallic Chemistry: Synthesis, Structure, and Reactivity of the Water-Soluble Metal Hydride $CpRu(PTA)_2H$. Organometallics 2004, 23, 5417–5323.
44. Nizomov N; Kholov AU; Ischenko AA; Ischenko VV; Khilya VP Electron Structure and Spectral Fluorescence Properties of Umbelliferone and Herniarin. J. Appl. Spec 2007, 74, 626–634.
45. Bureš F Fundamental Aspects of Property Tuning in Push–Pull Molecules. RSC Adv. 2014, 4, 58826–58851.

46. Lemieux GA; de Graffenried CL; Bertozzi CR A Fluorogenic Dye Activated by the Staudinger Ligation. J. Am. Chem. Soc 2003, 125, 4708–4709. [PubMed: 12696879]
47. Tirla A; Rivera-Fuentes P Development of a Photoactivatable Phosphine Probe for Induction of Intracellular Reductive Stress with Single-Cell Precision. Angew. Chem. Int. Ed 2016, 55, 14709–14712.
48. Hangauer MJ; Bertozzi CR A FRET-based Fluorogenic Phosphine for Live Cell Imaging with the Staudinger Ligation. Angew. Chem. Int. Ed 2008, 47, 2394–2397.
49. Friscourt F; Fahrni CJ; Boons GJ A Fluorogenic Probe for the Catalyst-Free Detection of Azide-Tagged Molecules. J. Am. Chem. Soc 2012, 134, 18809–18815. [PubMed: 23095037]
50. Favre C; Friscourt F Fluorogenic Sydnone-Modified Coumarins Switched-On by Copper-Free Click Chemistry. Org. Lett 2018, 20, 4213–4217. [PubMed: 29995429]
51. Hansch C; Leo A; Taft RW A Survey of Hammett Substituent Constants and Resonance and Field Parameters. Chem. Rev 1991, 91, 165–191.
52. Ni C; Hu J Recent Advances in the Synthetic Application of Diflurocarbene. Synthesis 2014, 46, 842–863.
53. Wang X; Liu Y; Fan X; Wang J; Ngai WSC; Zhang H; Li J; Zhang G; Lin J; Chen PR Copper-Triggered Bioorthogonal Cleavage Reactions for Reversible Protein and Cell Surface Modifications. J. Am. Chem. Soc 2019, 141, 17133–17141. [PubMed: 31580665]
54. McCourt RO; Dénès F; Sanchez-Sanz G; Scanlan EM Rapid Access to Thiolactone Derivatives through Radical-Mediated Acyl Thiol-Ene and Acyl Thiol-Yne Cyclization. Org. Lett 2018, 20, 2948–2951. [PubMed: 29717872]
55. Surry DS; Buchwald SL Dialkylbiaryl Phosphines in Pd-catalyzed Amination: a User's Guide. Chem. Sci 2011, 2, 27–50. [PubMed: 22432049]
56. Hundertmark T; Littke AF; Buchwald SL; Fu GC $Pd(PhCN)_2Cl_2/P(t\text{-}Bu)_3$: a Versatile Catalyst for Sonogashira Reactions of Aryl Bromides at Room Temperature. Org. Lett 2000, 2, 1729–1731. [PubMed: 10880212]
57. Dorel R; Echavarren AM Gold(I)-Catalyzed Activation of Alkynes for the Construction of Molecular Complexity. Chem. Rev 2015, 115, 9028–9072. [PubMed: 25844920]
58. Marchal E; Uriac P; Legouin B; Toupet L; van de Weghe P Cycloisomerization of γ- and δ-Acetylenic Acids Catalyzed by Gold (I) Chloride. Tetrahedron 2007, 63, 9979–9990.
59. Row RD; Prescher JA Constructing New Bioorthogonal Reagents and Reactions. Acc. Chem. Res 2018, 51, 1073–1081. [PubMed: 29727171]
60. Farrants H; Tarnawski M; Müller TG; Otsuka S; Hiblot J; Koch B; Kueblbeck M; Kräusslich HG; Ellenberg J; Johnsson K Chemogenetic Control of Nanobodies. Nat. Methods 2020, 17, 279–282. [PubMed: 32066961]
61. Hoelzel CA; Zhang X Visualizing and Manipulating Biological Processes by Using HaloTag and SNAP-tag Technologies. ChemBioChem 2020, 21, 1935–1946. [PubMed: 32180315]
62. Keppler A; Gendreizig S; Gronemeyer T; Pick H; Vogel H; Johnsson K A General Method for the Covalent Labeling of Fusion Proteins with Small Molecules *in vivo*. Nat. Biotechnol 2003, 21, 86–89. [PubMed: 12469133]
63. Flores J; White BM; Brea RJ; Baskin JM; Devaraj NK Lipids: Chemical Tools for their Synthesis, Modification, and Analysis. Chem. Soc. Rev 2020, 49, 4602–4614. [PubMed: 32691785]
64. Luu W; Sharpe LJ; Capell-Hattam I; Gelissen IC; Brown AJ Oxysterols: Old Tales, New Tricks. Annu. Rev. Pharmacol. Toxicol 2017, 56, 447–467.
65. Schroeder F; Huang H; McIntosh AL; Atshaves BP; Martin GG; Kier AB Caveolin, Sterol Carrier Protein-2, Membrane Cholesterol-rich Microdomains and Intracellular Cholesterol Trafficking. Subcell. Biochem 2010, 51, 279–318. [PubMed: 20213548]
66. Jean-Louis S; Akara S; Ali MA; Mash EA; Meuillet E; Martinez JD Deoxycholic Acid Induces Intracellular Signaling through Membrane Perturbations. J. Biol. Chem 2003, 281, 14948–14960.
67. Byrne AM; Sharma R; Duggan G; Kelleher D; Long A Deoxycholic Acid Impairs Glycosylation and Fucosylation in Esophageal Epithelial Cells. Glycobiology 2012, 22, 638–648. [PubMed: 22223758]

68. Májer F; Salomon JJ; Sharma R; Etzbach SV; Najib MMM; Keaveny R; Long A; Wang J; Ehrhardt C; Gilmer JF New Fluorescent Bile Acids: Synthesis, Chemical Characterization, and Diastereoselective Uptake by Caco-2 Cells of 3-Deoxy 3-NBC-amino Deoxycholic and Ursodeoxycholic Acid. Bioorg. Med. Chem. Lett 2012, 20, 1767–1778.
69. Gavin J; Quilty F; Majer F; Gilsenan G; Byrne AM; Long A; Radics G; Gilmer JF A Fluorescent Analogue of Tauroursodeoxycholic Acid Reduces ER Stress and is Cryoprotective. Bioorg. Med. Chem. Lett 2016, 26, 5369–5372. [PubMed: 27729186]
70. Hulce JJ; Cognetta AB; Niphakis MJ; Tully SE; Cravatt BF Proteome-wide Mapping of Cholestrol-Interacting Proteins in Mammalian Cells. Nat. Methods 2013, 10, 259–264. [PubMed: 23396283]
71. Cheng Y-S; Zhang Y; Ma X; Pratuangtham S; Zhang GC; Ondrus AA; Maji A; Lomenick B; Jones JJ; Ondrus AE A Proteome-wide Map of 20(S)-Hydeoxycholesterol Interactors in Cell Membranes. Nat. Chem. Biol 2021, 17, 1271–1280. [PubMed: 34799735]
72. Erdmann RS; Takakura H; Thompson AD; Rivera-Molina F; Allgeyer ES; Bewersdorf J; Toomre D; Schepartz A Super-resolution Imaging of the Golgi in Live Cells with a Bioorthogonal Ceramide Probe. Angew. Chem. Int. Ed 2014, 53, 10242–10246.
73. Byrne AM; Foran E; Sharma R; Davies A; Mahon C; O'Sullivan J; O'Donoghue D; Kelleher D; Long A Bile Acids Modulate the Golgi Membrane Fission Process via a Protein Kinase Cη and Protein Kinase D-Dependent Pathway in Colonic Epithelial Cells. Carcinogenesis 2010, 31, 737–744. [PubMed: 20093383]
74. Yang D; Yao M; Yan Y; Liu Y; Wen X; Chen X; Lu F Deoxycholic Acid Upregulates Serum Golgi Protein 73 through Activating NF-κB Pathway and Destroying Golgi Structure in Liver Disease. Biomolecules 2021, 11, 205. [PubMed: 33540642]
75. Bumpus TW; Baskin JM Greasing the Wheels of Lipid Biology with Chemical Tools. Trends Biochem. Sci 2018, 43, 970–983. [PubMed: 30472989]
76. Matikonda SS; Ivanic J; Gomez M; Hammersley G; Schnermann MJ Core Remodeling Leads to Long Wavelength Fluoro-Coumarins. Chem. Sci 2020, 11, 7302–7307. [PubMed: 34123014]
77. Gandioso A; Contreras S; Melnyk I; Oliva J; Nonell S; Velasco D; García-Amorós J; Marchán V Development of Green/Red-Absorbing Chromophores Based on a Coumarin Scaffold That Are Useful as Caging Groups. J. Org. Chem 2017, 82, 5398–5408. [PubMed: 28467700]
78. Gandioso A; Bresolí-Obach R; Nin-Hill A; Bosch M; Palau M; Galindo A; Contreras S; Rovira A; Rovira C; Nonell S; Marchán V Redesigning the Coumarin Scaffold into Small Bright Fluorophores with Far-Red to Near-Infrared Emission and Large Stokes Shifts Useful for Cell Imaging. J. Org. Chem 2018, 83, 1185–1195. [PubMed: 29283264]

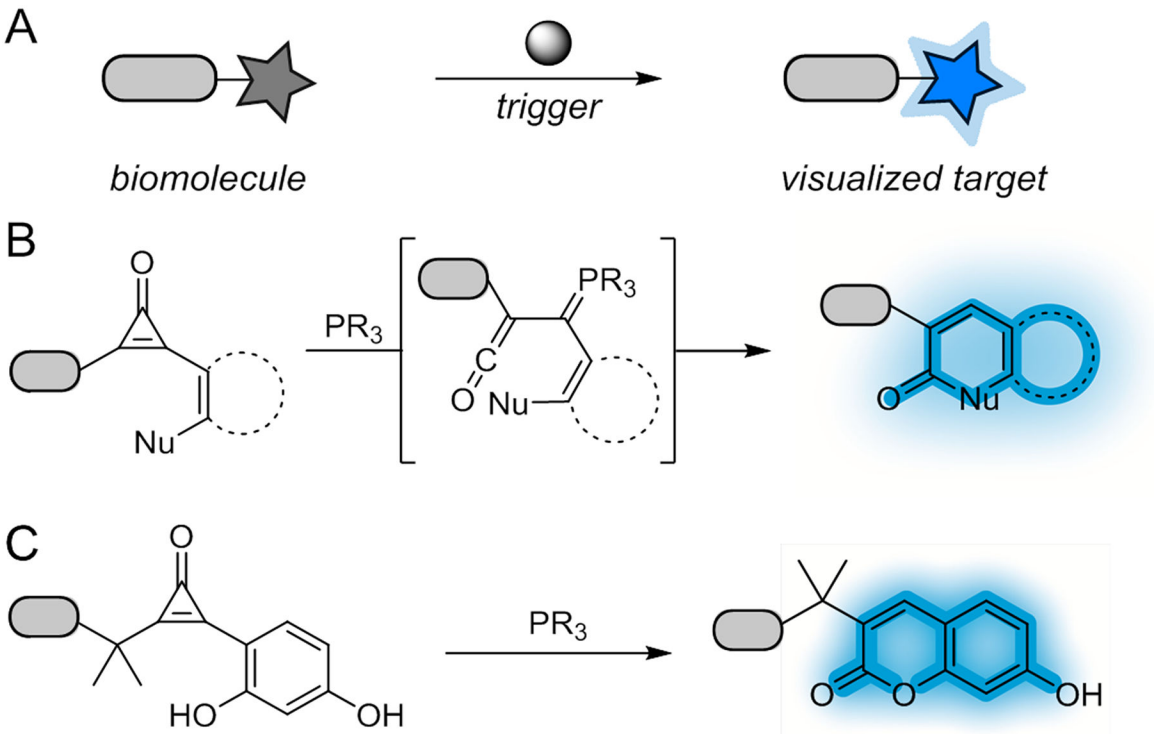

Figure 1.

Fluorogenic reactions for biomolecule visualization. (A) “Dark” reporters form fluorescent adducts upon treatment with a bioorthogonal chemical trigger. (B) Cyclopropenones react with phosphine catalysts to produce ketenes. These intermediates can be trapped by various nucleophiles to form cyclic products. (C) In this work, fluorogenic cyclopropenones were developed. These reporters react selectively with phosphine nucleophiles to form fluorescent hydroxycoumarins.

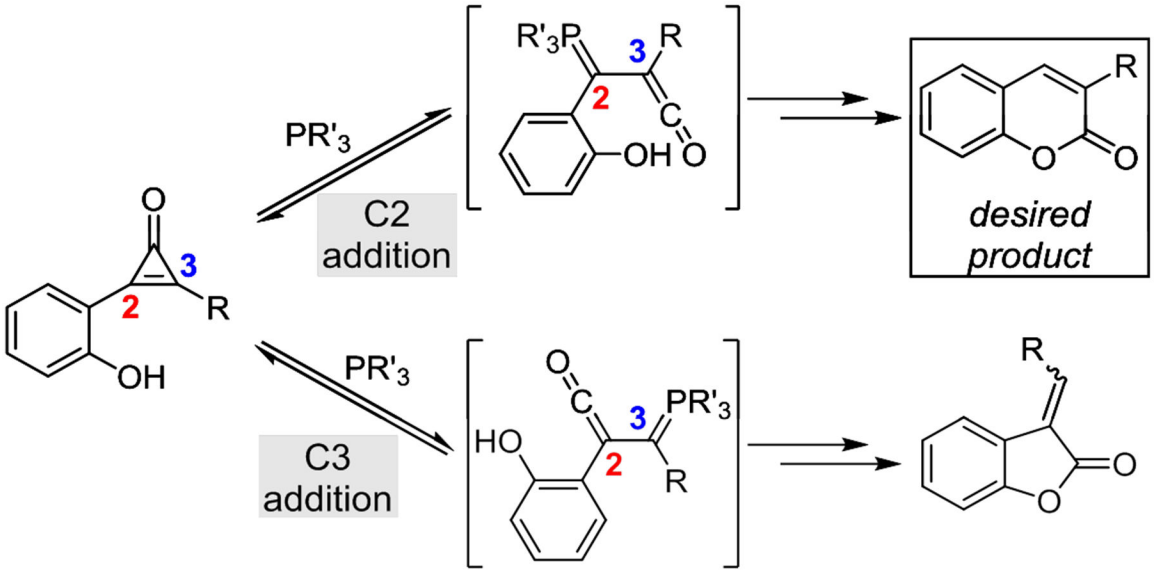

Figure 2.

Asymmetric CpOs can form two ketene-ylides upon phosphine treatment. Both intermediates react with pendent phenol nucleophiles to yield cyclized adducts. However, only phosphine addition at C2 yields the desired coumarin product; addition at C3 affords the undesired and non-fluorescent benzofuran-2(3H)-one adduct.

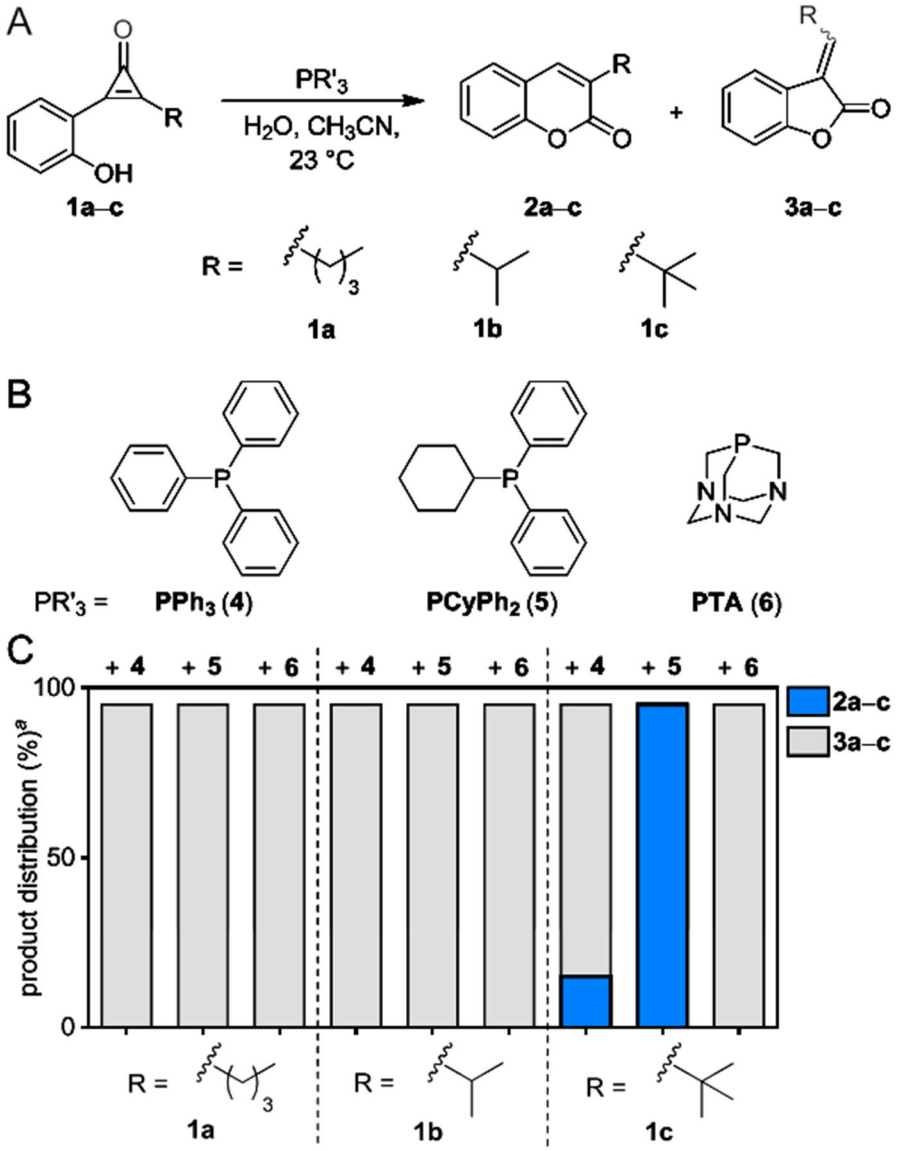

Figure 3.

Distinct regioisomers are formed upon CpO treatment with various phosphines. (A) Phosphine activation of sterically modified CpOs can provide two cyclized adducts. (B) Structures of the phosphine probes examined. (C) Product distributions from treatment of CpO **1a**–**c** with phosphines **4**–**6**. [a]Yields measured by ^{1}H-NMR spectroscopy.

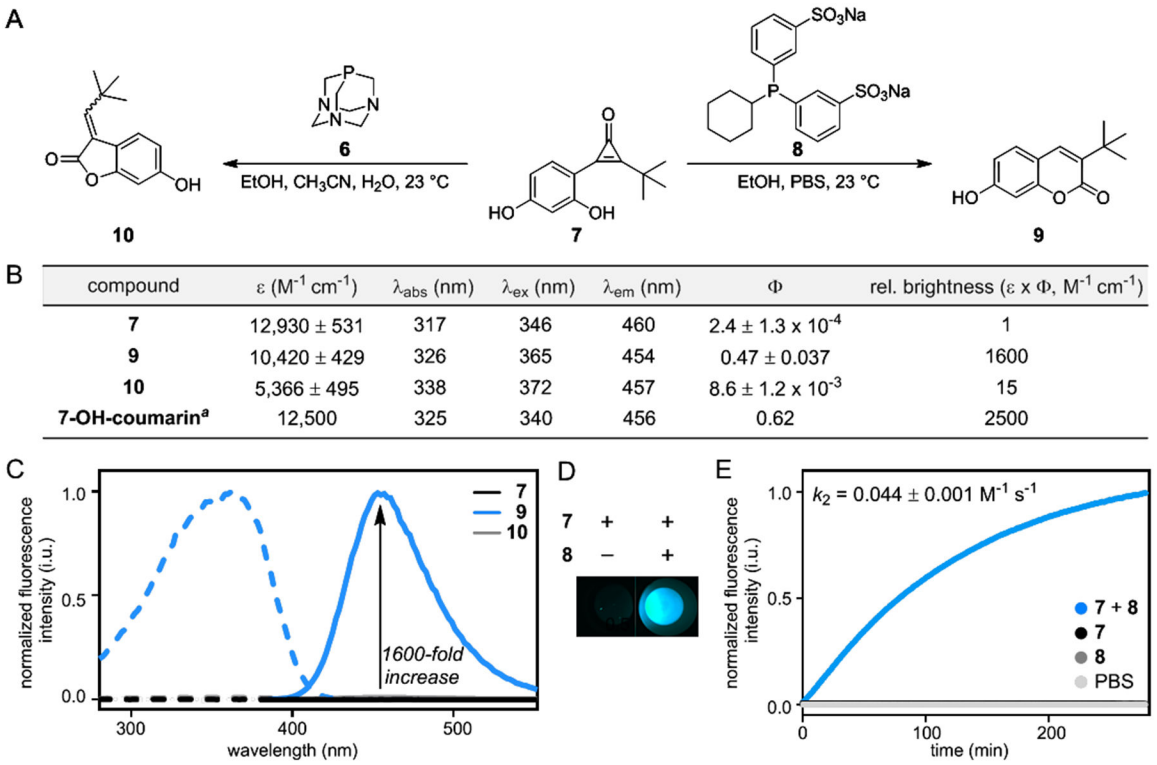

compound	ε (M^{-1} cm^{-1})	λ_{abs} (nm)	λ_{ex} (nm)	λ_{em} (nm)	Φ	rel. brightness (ε x Φ, M^{-1} cm^{-1})
7	12,930 ± 531	317	346	460	2.4 ± 1.3 x 10^{-4}	1
9	10,420 ± 429	326	365	454	0.47 ± 0.037	1600
10	5,366 ± 495	338	372	457	8.6 ± 1.2 x 10^{-3}	15
7-OH-coumarin[a]	12,500	325	340	456	0.62	2500

Figure 4.

Regioselective phosphine addition to CpOs yields fluorescent adducts. (A) Sterically occluded CpO **7** reacts with phosphine probes **6** or **8** to form two distinct products (**9**–**10**). (B) Photophysical properties of CpO **7** and adducts **9**–**10** (measured in 50% EtOH/PBS, pH 7.40). The fluorescence properties of cyclized product **9** are comparable to 7-hydroxycoumarin, an established fluorophore.[44] (C) Fluorescence spectra of CpO **7** and products **9**–**10** (10 μM, 50% EtOH/PBS, pH 7.40). Excitation spectra are shown in dashed lines, and emission spectra are shown in solid lines. (D) Fluorescence is dependent on the reaction of CpO **7** and phosphine **8**. (E) Kinetic analysis of the fluorogenic reaction. CpO **7** (100 μM) was reacted with phosphine probe **8** (5 mM) in PBS (pH 7.40), and coumarin fluorescence was monitored over time. [a]Measured in water.[44]

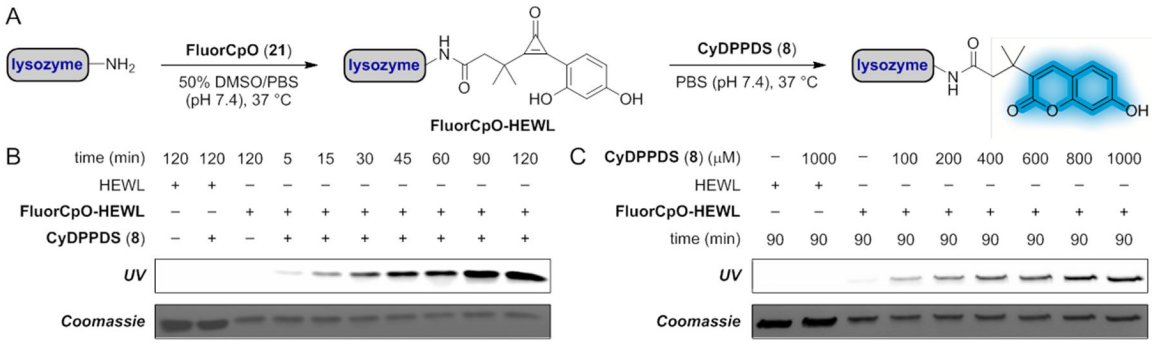

Figure 5.

The fluorogenic CpO-phosphine reaction labels protein targets *in vitro*. (A) **FluorCpO-HEWL** (1–6 modifications, Figure S11) was incubated with **CyDPPDS** to label protein conjugates. (B) SDS-PAGE analysis of **FluorCpO-HEWL** (40 μM) incubated with **CyDPPDS** (1 mM) for 5–120 min in PBS (pH 7.4). Fluorescent products were observed within 5 min. (C) SDS-PAGE analysis of **FluorCpO-HEWL** (40 μM) incubated with **CyDPPDS** (100–1000 μM) for 90 min in PBS (pH 7.4). Low concentrations of **CyDPPDS** (100 μM) were sufficient for fluorophore formation. Data are representative of three replicate experiments.

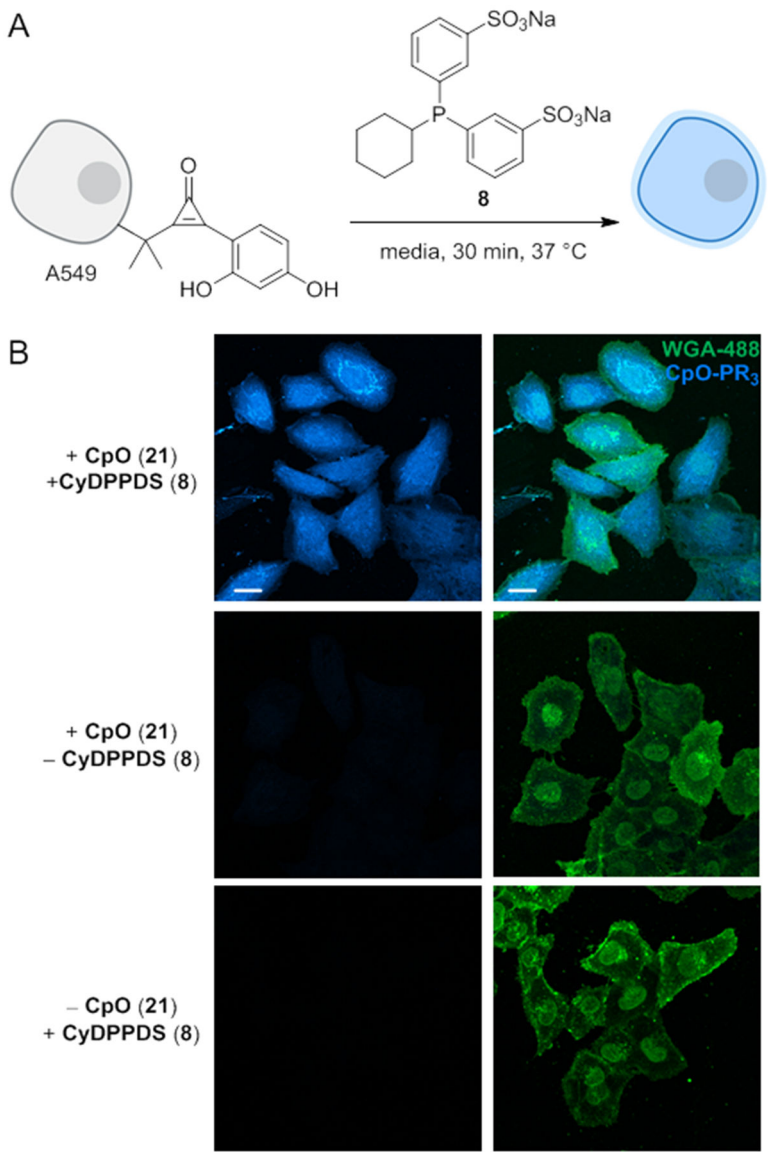

Figure 6.

The fluorogenic CpO-phosphine reaction can be performed on live cells. (A) A549 cells were non-specifically functionalized with CpO **21**. CpO-tagged biomolecules were then visualized upon treatment with phosphine **8**. (B) Coumarin fluorescence was only observed in the presence of both reagents. Cells surfaces were stained with a membrane marker to aid visualization (green channel, WGA-fluorescein conjugate). Data are representative of three replicate experiments. (Scale bar: 20 μm.)

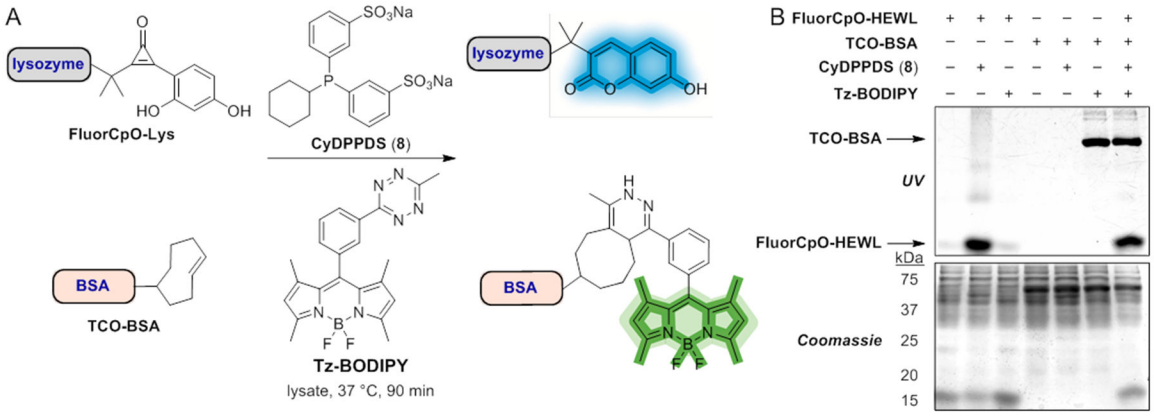

Figure 7.

Dual bioorthogonal fluorogenic reactions to simultaneously visualize protein targets. (A) Protein targets bearing **FluorCpO** or **TCO** handles were visualized in “one pot” fashion via reaction with complementary phosphine or tetrazine probes.[15] (B) Gel analysis of **FluorCpO-HEWL** (40 μM) and **TCO-BSA** (1 μM) reacted with **8** (10 mM) and **Tz-BODIPY** (100 μM) for 90 min in bacterial cell lysate (300 μg). Selective fluorophore formation was observed when both reactions were performed separately or together. Data are representative of three replicate experiments.

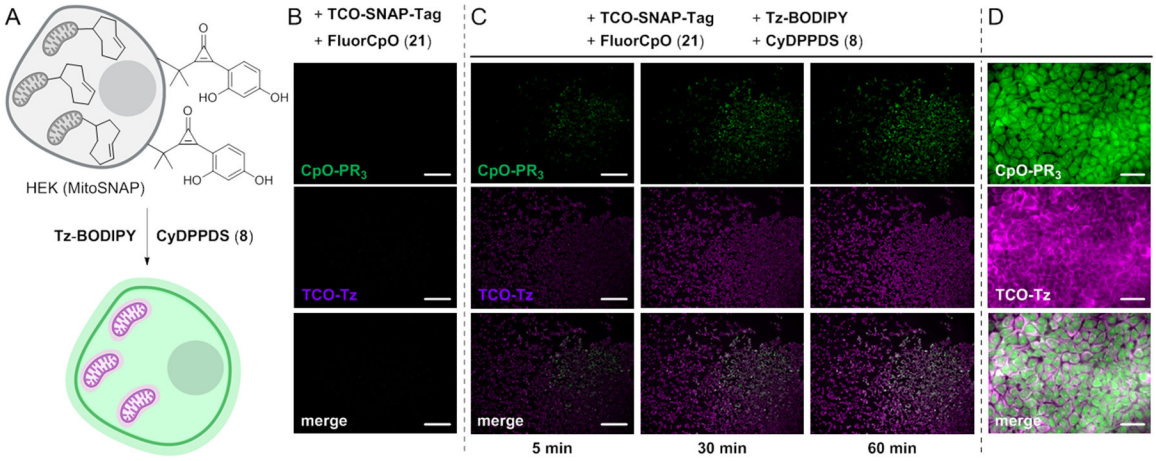

Figure 8.

Simultaneous two-color imaging using orthogonal fluorogenic chemistries in live cells. (A) HEK cells expressing a mitochondrial localized SNAP-tag protein were labeled with a **TCO-SNAP-tag** ligand (20 μM, 30 min, 37 °C). These cells were also nonspecifically conjugated with fluorogenic CpO **21** (1 mM, 15 min, 37 °C). To visualize modified biomolecules, **Tz-BODIPY** and **CyDPPDS** (**8**) probes were added (0.25 μM, 1 mM, respectively). The cells were imaged immediately after probe addition. (B) No background fluorescence was observed in the absence of the fluorogenic triggers, **Tz-BODIPY** and **CyDPPDS** (**8**). (Scale bar: 200 μm.) (C) Modified cells were reacted with **Tz-BODIPY** and **CyDPPDS** (**8**), enabling two-color visualization over 1 h. (Scale bar: 200 μm.) (D) High magnification images acquired after 90 min incubation. Data are representative of three replicate experiments. (Scale bar: 30 μm.)

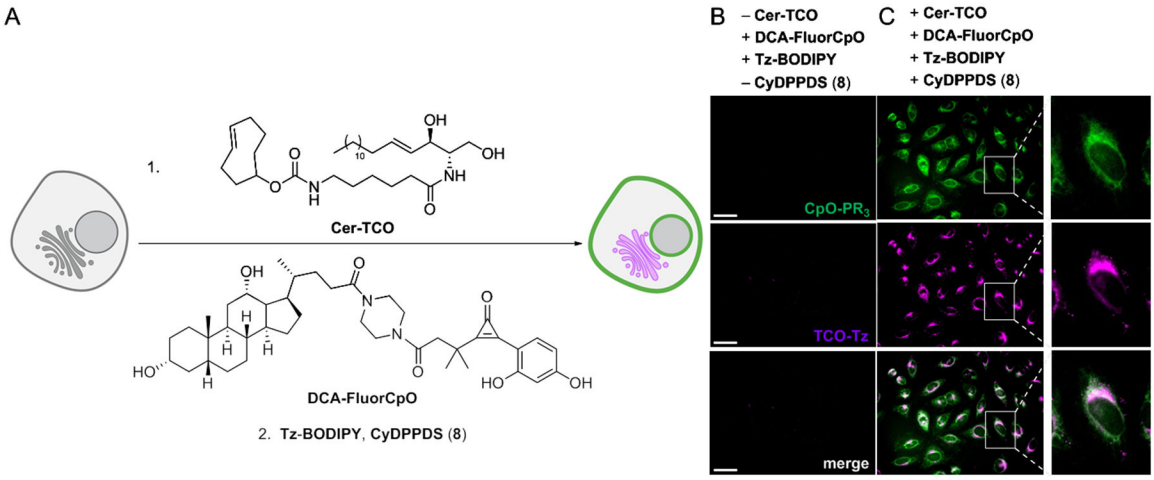

Figure 9.

Dual metabolite imaging with fluorogenic bioorthogonal chemistries. (A) **Cer-TCO** and **DCA-FluorCpO** were incubated with HeLa cells, prior to bioorthogonal detection. (B) No background labeling was observed in the absence of matched bioorthogonal pairs. (C) **Cer-TCO** and **DCA-FluorCpO** were visualized upon incubation with **Tz-BODIPY** and **CyDPPDS**. Data are representative of three replicate experiments. (Scale bars: 50 μm.)

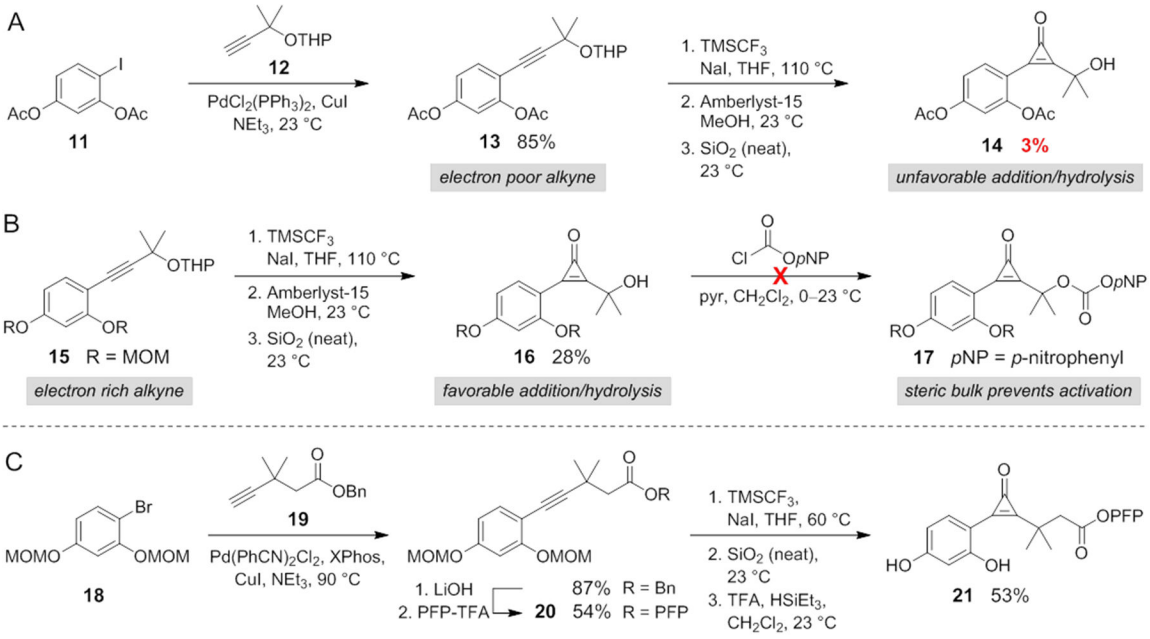

Scheme 1.

Synthesis of a fluorogenic CpO probe for bioconjugation.